Parameter dependence in the atmospheric decoherence of modal entangled photon pairs

Alpha Hamadou Ibrahim,[1,2] Filippus S. Roux,[1,*] and Thomas Konrad[2]

[1] *CSIR National Laser Centre, PO Box 395, Pretoria 0001, South Africa*
[2] *School of Physics, University of KwaZulu-Natal, Private Bag X54001, 4000 Durban, South Africa*

When a pair of photons that are entangled in terms of their transverse modes, such as an orbital angular momentum (OAM) basis, propagates through atmospheric turbulence, the scintillation causes a decay of the entanglement. Here, we use numerical simulations to study how this decoherence process depends on the various dimension parameters of the system. The relevant dimension parameters are the propagation distance, the wavelength, the beam radius and the refractive index structure constant, indicating the strength of the turbulence. We show that, beyond the weak scintillation regime, the entanglement evolution cannot be accurately modeled by a single phase screen that is specified by a single dimensionless parameter. Two dimensionless parameters are necessary to describe the OAM entanglement evolution. Furthermore, it is found that higher OAM modes are not more robust in turbulence beyond the weak scintillation regime.

PACS numbers: 03.65.Yz, 42.68.Bz, 03.67.Hk

I. INTRODUCTION

The orbital angular momentum (OAM) eigenstates of photons form an infinite-dimensional system. A superposition of $d > 2$ such states in a single photon encodes an amount of quantum information known as a *qudit* [1]. Photons that carry OAM are therefore a suitable candidate for applications such as quantum key distribution [2] with a larger alphabet [3]. As such, it is an attractive resource for the quantum information community.

Transmission through free-space can be used as a channel for high dimensional quantum communication. Unfortunately, unlike polarization, the OAM states of photons are severely affected by turbulence. Therefore, to use OAM modes successfully in free-space quantum communication, one needs to quantify and understand the effect of atmospheric turbulence on the OAM modes.

Most previous (theoretical and experimental) studies [4–8] of the effect of atmospheric turbulence on the modal entanglement of photon pairs are based on the single phase screen (SPS) approach [9], which uses a single phase screen to simulate the turbulent atmosphere. The random phase function of such a phase screen represents the phase modulation caused by the turbulence under weak scintillation conditions. The SPS approximation is therefore only valid for weak scintillation.

An alternative approach, which avoids the restriction of weak scintillation, is to use a multiple phase screen (MPS) approach. Recently, the MPS approach was used to derive first order differential equations that enable the study of turbulence-induced decoherence of entanglement encoded in the transverse spatial modes of photon pairs [10–12]. The MPS approach is valid in all scintillation conditions. According to [10], the parameter dependence in the atmospheric decoherence process is more complex than what is found from the SPS approach [9].

The aim of the present work is to use numerical simulations to investigate the parameter dependence of the atmospheric decoherence of photon pairs that are entangled in terms of their transverse spatial modes. We use the Kolmogorov theory of turbulence [13, 14] and restrict our numerical analyses to the two-level (qubit) case. The photons are assumed to be monochromatic, uniformly polarized and they propagate paraxially. Entanglement is quantified in terms of Wooter's concurrence [15].

The paper is organized as follows. First, we discuss the different parameters in Sec. II. The various technical aspects of the numerical simulations are explained in Sec. III. We address the validation of the numerical procedure in Sec. IV. The results that we obtain from these numerical simulations, which are presented and discussed in various ways in Sec. V, support the notion that in general two dimensionless parameters are needed to describe the atmospheric decoherence process. The conclusions are provided in Sec. VII.

II. PARAMETERS

The SPS approach is assumed to be valid when the irradiance fluctuations (scintillations) are weak. The scintillation strength is quantified by the Rytov variance, which is defined as

$$\sigma_R^2 = 1.23 C_n^2 k_0^{7/6} z^{11/6}, \tag{1}$$

where C_n^2 is the refractive index structure constant, z is the propagation distance and k_0 is the wavenumber. The condition for weak scintillation is $\sigma_R^2 < 1$ [14].

According to the SPS model, the effect of the turbulence on the entanglement of a photon pair is completely

*Electronic address: fsroux@csir.co.za

described by a single dimensionless parameter given by

$$\mathcal{W} = \frac{w_0}{r_0} \tag{2}$$

where w_0 is the radius of the optical beam and r_0 is the Fried parameter, which is given by

$$r_0 = 0.185 \left(\frac{\lambda^2}{C_n^2 z}\right)^{3/5}, \tag{3}$$

for plane waves within the Kolmogorov theory of turbulence [13, 14]. All the dimension parameters of the system (the beam radius w_0, the wavelength λ, the propagation distance z and the refractive index structure constant C_n^2) are combined into $\mathcal{W}$.

As we demonstrate below, the evolution of the decoherence process in the MPS approach requires at least two dimensionless parameter, instead of one. The two parameters are the normalized propagation distance

$$t = \frac{z}{z_R} = \frac{z\lambda}{\pi w_0^2}, \tag{4}$$

which is independent of the turbulent strength, and a system constant

$$\mathcal{K} = \frac{C_n^2 w_0^{11/3} \pi^3}{\lambda^3} = \frac{\mathcal{T}}{\theta_B^3}, \tag{5}$$

which is independent of the propagation distance. Here, $\mathcal{T} = C_n^2 w_0^{2/3}$ is a normalized turbulence strength and $\theta_B = \lambda/\pi w_0$ is the beam divergence angle. Note that the normalized propagation distance is related to the Fresnel number F by

$$t = \frac{1}{\pi F}. \tag{6}$$

According to [10], the MPS approach reverts back to the SPS approach [9] for $t \lesssim 1/3$ ($F \gtrsim 1$).

The three dimensionless parameters $\mathcal{W}$, $\mathcal{K}$ and t are related by

$$\mathcal{W} = 1.37 \mathcal{K}^{3/5} t^{3/5} \tag{7}$$

and the Rytov variance can also be expressed in terms of the dimensionless parameters as

$$\sigma_R^2 = 2.76 \mathcal{K} t^{11/6} = 1.64 \mathcal{W}^{5/3} t^{5/6}. \tag{8}$$

III. NUMERICAL PROCEDURE

A. Input functions

The quantum optical system that is simulated by our numerical procedure, is shown in Fig. 1. The source generates a pair of photons that are initially in a maximally OAM entangled state. The OAM basis states $|\ell, p\rangle$ correspond to elementary excitations of the LG modes $M_{\ell p}^{\mathrm{LG}}(r, \phi, t)$ of the electromagnetic fields, which can be expressed in normalized cylindrical coordinates by

$$M_{\ell p}^{\mathrm{LG}}(r, \phi, t) = \mathcal{N} \frac{r^{|\ell|} \exp(\mathrm{i}\ell\phi)(1 + \mathrm{i}t)^p}{(1 - \mathrm{i}t)^{p+|\ell|+1}} \times L_p^{|\ell|}\left(\frac{2r^2}{1+t^2}\right) \exp\left[-\frac{r^2}{1 - \mathrm{i}t}\right], \tag{9}$$

were $L_p^{|\ell|}$ represents the generalized Laguerre polynomials with the parameters ℓ and p being the azimuthal and the radial mode indices, respectively; $r = (x^2 + y^2)^{1/2}/w_0$, ϕ is the azimuthal angle and z_R is the Rayleigh range ($= \pi w_0^2/\lambda$). The normalization constant is given by

$$\mathcal{N} = \left[\frac{p! 2^{|\ell|+1}}{\pi (p + |\ell|)!}\right]^{1/2}. \tag{10}$$

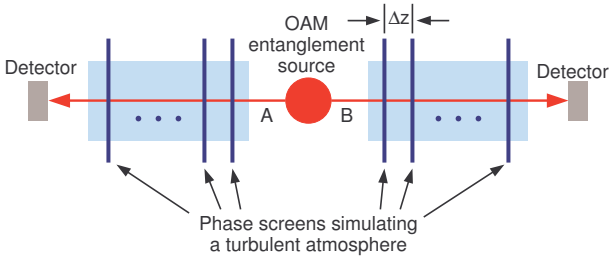

FIG. 1: The source generates two photons that are entangled in OAM. Each photon is then sent through a turbulent atmosphere (modeled by a series of phase screens) toward a detector.

The initial quantum state in the numerical simulations is a Bell state

$$|\Psi\rangle_{in} = \frac{1}{\sqrt{2}} \left(|\ell\rangle_A |-\ell\rangle_B + |-\ell\rangle_A |\ell\rangle_B\right), \tag{11}$$

where the subscripts A and B label the two different paths of the two photons through turbulence. We only consider the zero radial index $p = 0$ and azimuthal indices of $\ell = 1, 3, 5, 7$ in our simulations.

The initial state requires four optical fields that correspond to the two possible states of each of the two photons labeled by A and B in Eq. (11). Each optical field is represented by a 256×256 array of samples of the complex-valued function for the mode given in Eq. (9).

B. The split-step method

The evolution of the quantum state of the two qubits, starting from the initial state given in Eq. (11), is determined by simulating the propagation of the four optical fields through turbulence. As a result, four propagations are required for each realization of the turbulent media.

The two photons respectively propagate through different uncorrelated turbulent media, as denoted by the two propagation paths indicated by A and B in Fig. 1.

The refractive index n of a turbulent medium is inhomogeneous and can be represented by

$$n = 1 + \delta n(\mathbf{x}), \tag{12}$$

indicating that the average refractive index of air is taken as 1, while the fluctuation is given by $\delta n(\mathbf{x})$ and is very small ($\delta n \ll 1$). We assume that the beam propagates paraxially, which leads to the paraxial wave equation with an extra inhomogeneous medium term [14]

$$\nabla_T^2 g(\mathbf{x}) - i2k_0\partial_z g(\mathbf{x}) + 2k_0^2\delta n(\mathbf{x})g(\mathbf{x}) = 0, \tag{13}$$

where (assuming that the paraxial beam propagates in the z-direction and is uniformly polarized)

$$E(\mathbf{x}) = g(\mathbf{x})\exp(-ik_0 z) \tag{14}$$

is the scalar part of the electric field, ∇_T is the transverse part of the gradient operator and $\mathbf{x}$ is a three-dimensional position vector.

Due to the smallness of $\delta n(\mathbf{x})$ compared to the average refractive index, the modulation by the refractive index fluctuation separates from the free-space propagation in Eq. (13). This suggests that one can model the propagation through turbulence by a repeated two-step process that alternates the modulation of the beam by the random phase fluctuation and the propagation of the beam over a short distance through free-space without turbulence. The numerical technique that is based on this approach is known as the split-step method or the phase screen method [16, 17]. In this method, the atmosphere is represented by a series of phase screens separated by a distance Δz as shown in Fig. 1.

Each phase screen contains a random phase function that represents a layer of turbulent atmosphere with a thickness of Δz. This phase function can be expressed in terms of the refractive index fluctuation of the medium

$$\theta(x,y) = k_0\int_0^{\Delta z}\delta n(x,y,z)\mathrm{d}z. \tag{15}$$

Each phase screen imparts a random phase modulation on the phase of the optical beam passing through it. After the phase screen, the beam propagates through free-space (without turbulence) over a distance Δz between consecutive phase screens. During propagation the phase distortion induces an amplitude distortion on the beam.

The properties of the random fluctuations of the refractive index is determined by the properties of the turbulent medium. Within the Kolmogorov theory, these properties are given by the power spectral density of the refractive index fluctuation

$$\Phi_n(\mathbf{k}) = 0.033C_n^2|\mathbf{k}|^{-11/3}, \tag{16}$$

where $\mathbf{k}$ is the three-dimensional coordinate vector in the Fourier domain and C_n^2 is the refractive index structure constant. The Kolmogorov theory is valid over the inertial range $1/L_0 \ll |\mathbf{k}| \ll 1/l_0$, where L_0 and l_0 are the outer and inner scales, respectively. In the simulation, these cut-offs are set by the smallest grid spacing in the Fourier domain and the overall size of the angular spectrum, respectively.

The expression of the random phase in terms of the power spectral density of the refractive index fluctuations, is given by [8, 16, 17]

$$\begin{aligned}\theta(x,y) &= \frac{k_0}{\Delta_k}(2\pi\Delta z)^{1/2} \\ &\quad\times\mathcal{F}^{-1}\left\{\xi(k_x,k_y)\left[\Phi_n(k_x,k_y,0)\right]^{1/2}\right\},\end{aligned} \tag{17}$$

where $\mathcal{F}^{-1}$ is the two-dimensional inverse Fourier transform, $\xi(k_x,k_y)$ is a zero-mean normally distributed random complex-valued function and Δ_k is the spacing between samples in the frequency domain. The square root of the power spectral density of the phase function gives the envelope of the Fourier transform of the random phase function on a phase screen. The randomness is added by multiplying the envelop by $\xi(k_x,k_y)$. Note that the phase function thus generated is complex-valued $\theta(x,y) = \theta_1(x,y) + i\theta_2(x,y)$. This has the advantage that the real and imaginary parts of the complex-valued phase function can be used for two phase screens after each calculation, having transmission functions $t_1 = \exp(\mathrm{i}\theta_1)$ and $t_2 = \exp(\mathrm{i}\theta_2)$, respectively.

The free-space propagation is done by first computing the angular spectrum $G(k_x,k_y)$ of the beam profile at a specific value of z (say $z = 0$)

$$G(k_x,k_y) = \mathcal{F}\left\{g(x,y,0)\right\}, \tag{18}$$

where $\mathcal{F}$ denotes the two-dimensional Fourier transform. The angular spectrum is multiplied by a phase function for the change in phase incurred by each plane wave after propagating a distance Δz. Finally, the beam is reconstructed at $z = \Delta z$ by the inverse Fourier transform

$$g(x,y,\Delta z) = \mathcal{F}^{-1}\{G(k_x,k_y)\exp[-\mathrm{i}\Delta z k_z(k_x,k_y)]\}, \tag{19}$$

where $k_z(k_x,k_y) = \left(k_0^2 - k_x^2 - k_y^2\right)^{1/2}$.

The propagation is simulated by the split-step method where we start with the phase modulation by the random phase function of the phase screen, as computed with Eq. (17). Then the resulting four beam profiles are propagated through free-space over a distance of Δz, as expressed in Eq. (18) and Eq. (19). These two steps (the random phase modulation and the free-space propagation) are repeated several times, for different random phase functions, using the four distorted beam profiles obtained from the previous two steps, until the beams have propagated far enough to have lost their entanglement. Different values of the turbulence strength C_n^2, the beam waist radius w_0 and the wavelength λ are used in

the simulations (see Table I). Since the overall propagation distances in the simulations can vary quite drastically as a function of the different parameters, different values of Δz are used in different simulations. Depending on the parameters, the total propagation distance may range from less than a kilometer to several kilometers.

C. Data extraction

After the two photons propagated through the turbulent media, they are analyzed in detectors, which perform a state tomography to determine the density matrix of the bi-photon quantum state. In the simulations, the state tomography is performed after each iteration.

Although the OAM Hilbert space is infinite, we only extract the two-level quantum information (qubits) in this work. The basis of our two-level Hilbert space is

$$\mathcal{B} = \{|-\ell,-\ell\rangle, |-\ell,\ell\rangle, |\ell,-\ell\rangle, |\ell,\ell\rangle\}, \tag{20}$$

where $\ell = 1, 3, 5$ or 7.

When a photon carrying OAM propagates in a turbulent atmosphere, the refractive index fluctuations cause the OAM state of the photon to become scattered into neighboring OAM modes. That is, the initial OAM state of the photon will become a superposition of many OAM states [8]. However, since we only consider qubits here, we extract only the informations contained in the basis $\mathcal{B}$. Thus, after propagating through turbulence, the initial state given in Eq. (11) becomes

$$\begin{aligned} |\Psi\rangle_{\text{in}} \rightarrow |\Psi\rangle_{\text{out}} \;&=\; C_1|-\ell,-\ell\rangle + C_2|-\ell,\ell\rangle \\ &\quad + C_3|\ell,-\ell\rangle + C_4|\ell,\ell\rangle, \end{aligned} \tag{21}$$

where C_i represents the complex coefficients in the expansion of the distorted state in terms of the qubit basis in Eq. (20) [8]. This process occurs for each iteration in the simulation. Note that, since the complete field (as a pure state) is propagated through all the phase screens, the simulation incorporates all the transverse modes that can be represented by the resolution in the simulation.

The density matrix $|\Psi\rangle_{\text{out}}\langle\Psi|_{\text{out}}$, obtained from Eq. (21), is that of a pure state representing the two qubits for a specific realization of the turbulent medium. Because of the randomness of the medium, one would get a different density matrix for another realization of the medium. Thus, to obtain an accurate description of the evolution of the state of the two qubits, one needs to compute the ensemble average of the density matrices corresponding to all possible (or a representative set of) realizations of the medium. More explicitly, the density matrix that is obtained after each iteration in the simulation, is calculated by

$$\rho = \frac{\sum_n^N |\Psi_n\rangle\langle\Psi_n|}{\text{Tr}\left\{\sum_n^N |\Psi_n\rangle\langle\Psi_n|\right\}}, \tag{22}$$

for N different instances of the medium.

We quantify the entanglement between the two qubits with the concurrence [15]. It is defined by

$$\mathcal{C}(\rho) = \max\{0, \sqrt{\lambda_1} - \sqrt{\lambda_2} - \sqrt{\lambda_3} - \sqrt{\lambda_4}\}, \tag{23}$$

with λ_i being the eigenvalues in decreasing order of the Hermitian matrix

$$R = \rho(\sigma_y \otimes \sigma_y)\rho^*(\sigma_y \otimes \sigma_y), \tag{24}$$

where * represents the complex conjugate and σ_y is the Pauli y-matrix

$$\sigma_y = \begin{bmatrix} 0 & -\text{i} \\ \text{i} & 0 \end{bmatrix}. \tag{25}$$

The coefficients of the different modes are extracted from the four beam profiles after each free-space propagation step. The output quantum state is then computed from these coefficients, as described by Eq. (21), and the corresponding density matrix is determined. This sequence of density matrices, obtained during one run of the simulation, represents the evolution of the quantum state for a specific set of phase screens or a specific realization of the medium. We performed a number of $N = 1000$ such runs corresponding to N different simulated instances of the turbulent medium to obtain N different evolutions of the quantum state. The final sequence of density matrices is then computed from the ensemble averages of the N sequences obtained from these N runs, as described by Eq. (22).

IV. VALIDITY OF THE SIMULATION

We validate our simulation procedure by considering the formula, derived in [18], stating that the entanglement reduction induced by a one-sided noisy channel is independent of the initial state and completely determined by the channel's action on a maximally entangled state (see also [19–21]). One can express the formula by

$$\mathcal{C}_{\text{out}} = \mathcal{C}_{\text{ch}}\mathcal{C}_{\text{in}}, \tag{26}$$

where the input state $|\chi\rangle$ is a partially entangled pure state with a concurrence [15] given by $\mathcal{C}_{\text{in}} = \mathcal{C}(|\chi\rangle\langle\chi|)$; the concurrence of the channel $\mathcal{C}_{\text{ch}} = \mathcal{C}[(I \otimes \$)|\Psi\rangle\langle\Psi|]$ is determined by having the one-sided noisy channel $(I \otimes \$)$ operate on a maximally entangled (Bell) state $|\Psi\rangle$; and the output concurrence $\mathcal{C}_{\text{out}} = \mathcal{C}[(I \otimes \$)|\chi\rangle\langle\chi|]$ is determined by having the one-sided channel operate on the input state.

The one-sided channel in our case corresponds to the situation where only one of the two photons propagates through turbulence, as illustrated in Fig 2. The two sides of Eq. (26) are compared in Fig. 3, where we use the following partially entangled pure input state

$$|\chi\rangle = \frac{1}{2}|\ell\rangle_A|-\ell\rangle_B + \sqrt{\frac{3}{4}}|-\ell\rangle_A|\ell\rangle_B. \tag{27}$$

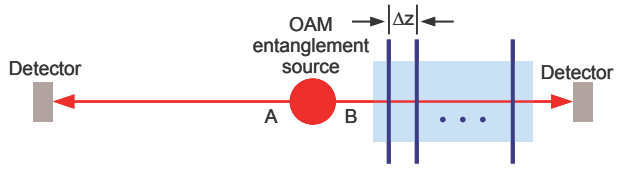

FIG. 2: The one-sided channel ($I \otimes \$$) where only one of the two photons propagates through turbulence.

It is clear that the evolution of $\mathcal{C}_{\rm out}$ is equal to $\mathcal{C}_{\rm ch}\mathcal{C}_{\rm in}$ over the entire range of $\mathcal{W} = w_0/r_0$ up to where the concurrence becomes zero.

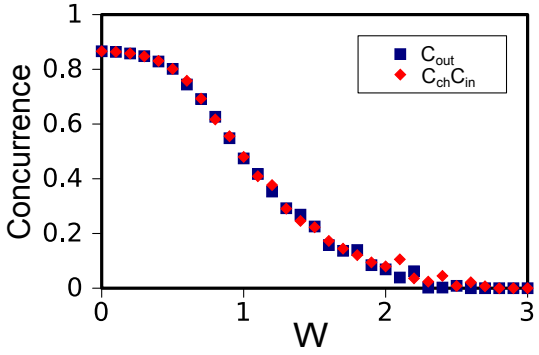

FIG. 3: Comparison of $\mathcal{C}_{\rm out}$ and $\mathcal{C}_{\rm ch}\mathcal{C}_{\rm in}$ as a function of $\mathcal{W}$.

Alternatively, for a fixed propagation distance, the output entanglement (concurrence) that is obtained after various partially entangled pure input states propagated through the one-sided channel, would be linearly related to the concurrence of the input state. The slope of the linear relationship is given by $\mathcal{C}_{\rm ch}$ for the fixed value of z. In Fig. 4 we plot $\mathcal{C}_{\rm out}$ against $\mathcal{C}_{\rm in}$ for eight different initial states of the form

$$|\chi\rangle_n = \sqrt{\frac{1}{n}}|\ell\rangle_A|-\ell\rangle_B + \sqrt{1-\frac{1}{n}}|-\ell\rangle_A|\ell\rangle_B, \qquad (28)$$

for $n = 3, 4, 5, \cdots 10$. Each point in Fig. 4 is averaged over 500 realizations of the turbulent medium.

Based on the results presented in Figs. 3 and 4, we conclude that it is reasonable to use the presented numerical procedure to study the evolution of OAM entanglement in the atmosphere.

V. NUMERICAL RESULTS

A. Effect of the system constant $\mathcal{K}$

Various simulations with different sets of parameters were performed to investigate the effect of the system constant $\mathcal{K}$ on the evolution of OAM entanglement in turbulence. (In Sec. V E below, we demonstrate that

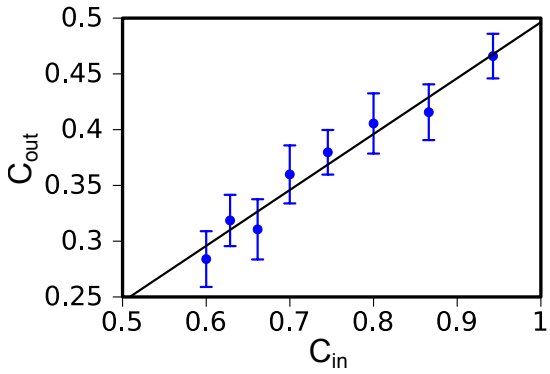

FIG. 4: Plot of $\mathcal{C}_{\rm out}$ against $\mathcal{C}_{\rm in}$ for eight different initial states. The error bars represent the dispersion of each run from the mean.

the evolution of the concurrence is invariant with respect to variations in the dimension parameters that produce the same value of $\mathcal{K}$.) Figure 5 shows the plots of the concurrence against $\mathcal{W}$ for different values of $\mathcal{K}$ and for $\ell = 1, 3, 5, 7$. The different sets of dimension parameters that were used to produce the different values of $\mathcal{K}$ [according to Eq. (5)] are given in Table I. Note that we deliberately used various different values of w_0, λ and C_n^2 to produce the different values of the system constant $\mathcal{K}$.

The general trend in the decay of the concurrence as a function of $\mathcal{W}$ is qualitatively the same for all the ℓ-values considered. For large values of $\mathcal{K}$, the concurrence lies on a limiting curve as a function of $\mathcal{W}$, but tends to lie below this limiting curve when $\mathcal{K}$ is small. The limiting curve is close to the theoretical curve obtained from the SPS approach, which is represented by the solid line curves in Fig. 5. One can see that there is a value of $\mathcal{K}$ beyond which the evolution of the concurrence depends only on $\mathcal{W}$. According to the curves in Fig. 5 the limiting curves are obtained when $\mathcal{K} \gtrsim 10$ for $\ell = 1, 3$, $\mathcal{K} \gtrsim 20$ for $\ell = 5$, and $\mathcal{K} \gtrsim 100$ for $\ell = 7$. The limiting curve corresponds to the situation that is considered in the SPS approach [4, 9], where the behavior is completely determined by $\mathcal{W}$ [4, 8, 10].

On the other hand, for small values of $\mathcal{K}$ (i.e., when $\mathcal{K} \lesssim 5$ for $\ell = 1, 3$; $\mathcal{K} \lesssim 10$ for $\ell = 5$; and $\mathcal{K} \lesssim 30$ for $\ell = 7$), the concurrence deviates from the limiting curve — it decays faster than the limiting curve as a function $\mathcal{W}$. This deviation implies that the SPS approach cannot be used under these conditions. Instead, two dimension parameters ($\mathcal{K}$ and t) are required to describe the evolution of the concurrence under these conditions.

B. Effect of the normalized propagation distance t

It was previously found [10] that the evolution of the concurrence cannot be fully described by the single parameter $\mathcal{W}$ when the concurrence survives for a distance larger than the Rayleigh range. To see at what value

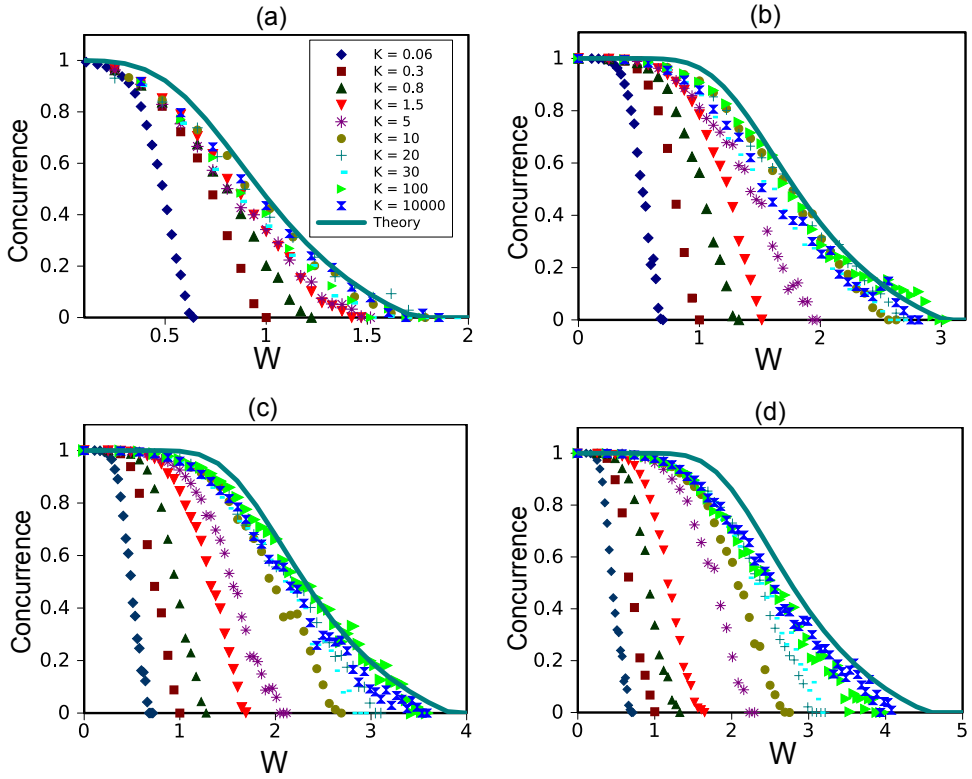

FIG. 5: The concurrence against $\mathcal{W}$ for (a) $\ell = 1$, (b) $\ell = 3$, (c) $\ell = 5$ and (b) $\ell = 7$. Each graph contains curves for all the different values of $\mathcal{K}$ given in Table I.

TABLE I: Dimension parameters for the different values of the system constant $\mathcal{K}$ shown in Fig. 5.

$\mathcal{K}$	w_0 (m)	C_n^2 ($\mathrm{m}^{-2/3}$)	λ (nm)
0.06	0.10	1.0×10^{-17}	1000
0.3	0.05	1.0×10^{-17}	1414
0.8	0.10	2.5×10^{-17}	600
1.5	0.10	5.0×10^{-17}	600
5	0.20	5.0×10^{-17}	947
20	0.10	1.0×10^{-16}	322
30	0.20	9.7×10^{-16}	1400
10^2	0.05	3.2×10^{-13}	1190
10^4	0.10	5.0×10^{-12}	1495

of t the curves in Fig. 5 start to deviate from the limiting curve, we calculate the difference in the concurrence between the theoretical SPS curve (solid line curves in Fig. 5) and the numerical curves that are shown in Fig. 5. In other words, we calculated $\Delta\mathcal{C} = \mathcal{C}_{\text{th}} - \mathcal{C}_{\text{num}}$ for all the different values of $\mathcal{K}$ given in Table I. The results are plotted against t in Fig. 6.

Those values of $\mathcal{K}$ that produce limiting curves represent cases where the concurrence becomes zero before the propagation distance reaches $t = 0.1$. We see in Fig. 6 that the difference $\Delta\mathcal{C}$ remains small (< 0.2) up to about $t = 0.1$. The value of $\Delta\mathcal{C}$ for the large values of $\mathcal{K}$ should be zero, but because the numerical limiting curves do not exactly match the theoretical (SPS) curve, we see that the difference in the concurrence shown in Fig. 6 is not exactly zero, but can be as large as 0.2. The reason for the difference between the numerical limiting curves and the theoretical curve is believed to be due to the fact that the theoretical SPS calculations employ the quadratic approximation to the structure function of the refractive index fluctuations [14, 22] in order to solve the overlap integrals from which the concurrence is computed [4]. On the other hand, the numerical simulations do not use the quadratic approximation.

The end points of the curves represent the points where the concurrence in the simulation becomes zero. We observe from the locations of these points in Fig. 6 that the concurrence survives up to increasing values of t as the value of $\mathcal{K}$ becomes smaller. Furthermore, one sees that for smaller values of $\mathcal{K}$, the curves start to deviate significantly from the limiting curves. These deviations start at a value of $t = z/z_R$ between 0.1 and 1.

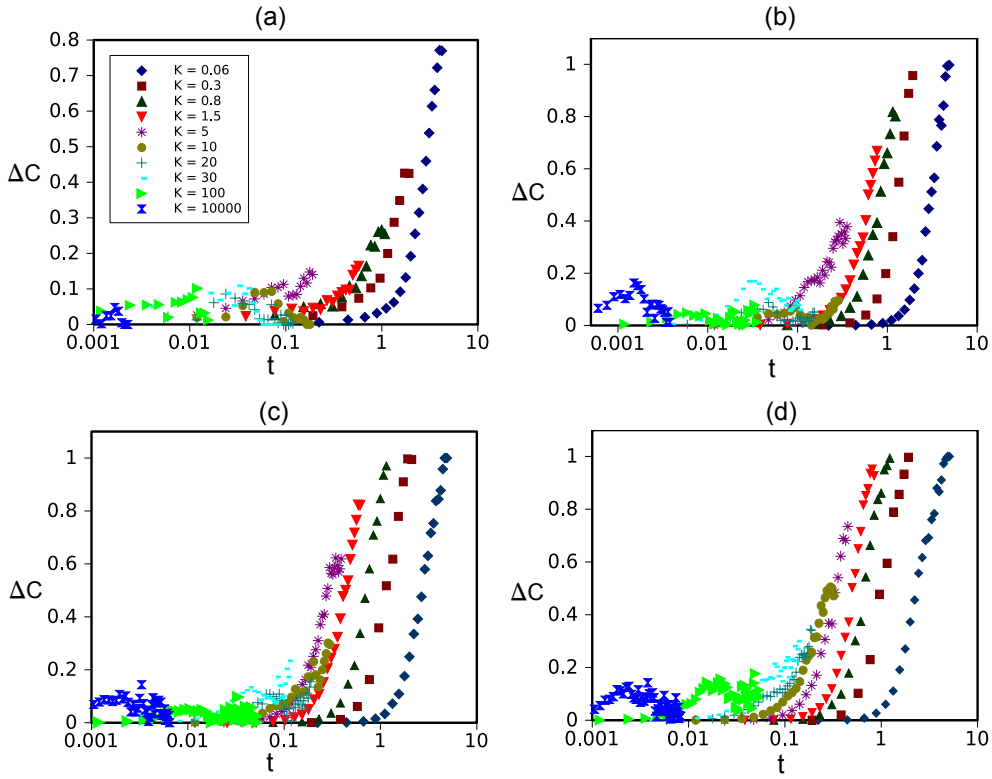

FIG. 6: The difference in the concurrence $\Delta\mathcal{C} = \mathcal{C}_{\rm th} - \mathcal{C}_{\rm num}$ against the normalized propagation distance t for (a) $\ell = 1$, (b) $\ell = 3$, (c) $\ell = 5$ and (d) $\ell = 7$. Each graph contains curves for all the different values of $\mathcal{K}$ given in Table I.

C. Effect of the Rytov variance σ_R^2

Scintillation regimes (weak or strong) are usually indicated by the value of the Rytov variance σ_R^2, given in Eq. (1). Weak scintillation conditions are said to exist when $\sigma_R^2 < 1$ [14]. To determine the scintillation strength where the concurrence curves start to deviate from the theoretical limiting curve, we plot in Fig. 7 the difference in the concurrence $\Delta\mathcal{C} = \mathcal{C}_{\rm th} - \mathcal{C}_{\rm num}$ as a function of the Rytov variance. Two significant observations can be made from Fig. 7. Firstly, the deviations start to occur at $\sigma_R^2 \approx 0.3$, which implies that the SPS approach breaks down at a scintillation strength of about $\sigma_R^2 = 0.3$. Secondly, the end points of the curves, which represent the points where the concurrence goes to zero, all appear at or before $\sigma_R^2 \approx 3$. This observation indicates that the concurrence cannot survive when the scintillation becomes stronger than about $\sigma_R^2 = 3$.

In other words, all the curves that fall on the limiting curve in Fig. 5 represent the evolution of the OAM entanglement in the weak fluctuation regime where $\sigma_R^2 < 0.3$. One can, therefore, conclude that the evolution of the OAM entanglement can only be fully described by the single dimensionless quantity $\mathcal{W} = w_0/r_0$ as long as scintillation remains weak, i.e., $\sigma_R^2 < 0.3$. In the region where $0.3 < \sigma_R^2 < 3$ the evolution curves deviate from the limiting curve, which represents the single parameter SPS approach. Hence, in this region of scintillation strength, two dimensionless parameters are required to described the evolution of the concurrence.

D. Effect of the azimuthal index ℓ

We now consider the effect of the azimuthal index ℓ on the evolution of the concurrence. For this purpose we show in Fig. 8 the concurrence as functions of $\mathcal{W}$ and t for $\ell = 1, 3, 5, 7$ and for $\mathcal{K} = 0.06, 10, 100$. We start with the largest value of $\mathcal{K}$ in Fig. 8(a), because it represents the limiting curves.

For $\mathcal{K} = 100$, shown in Fig. 8(a), all the curves for the concurrence decay to zero before they reach the value $t = 0.1$. As a result these curves all lie on their respective limiting curves for the different values of ℓ. As such these curves only depend on $\mathcal{W}$. For larger values of ℓ (larger amounts of OAM per photon) the entanglement survives longer, reaching larger values of both $\mathcal{W}$ and t. Under these conditions, entangled photon pairs composed of higher OAM modes are more robust against atmospheric decoherence. The same behavior was observed previously [4, 8, 10].

In Fig. 8(b), which shows the curves for $\mathcal{K} = 10$, we see that the curves for $\ell = 3, 5, 7$ have merged almost completely. These three curves extend beyond the $t = 0.1$ point, but they decay to zero at smaller values of $\mathcal{W}$, which means that they lie below the limiting curve (see

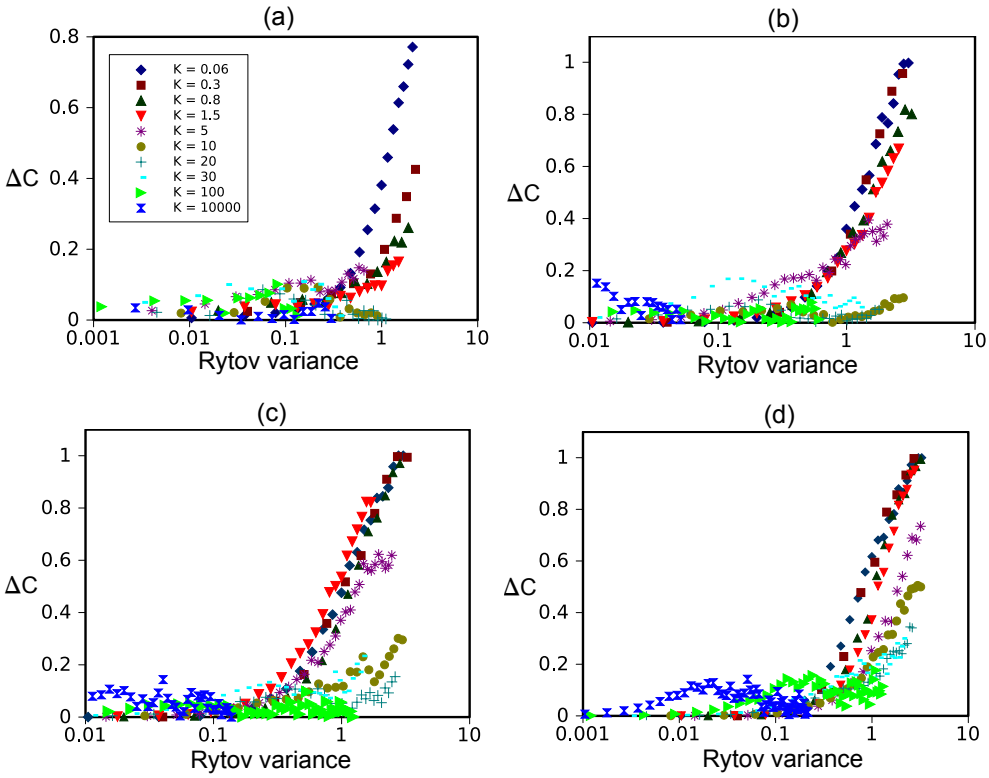

FIG. 7: The difference in the concurrence $\Delta\mathcal{C} = \mathcal{C}_{\rm th} - \mathcal{C}_{\rm num}$ against the Rytov variance σ_R^2 for (a) $\ell = 1$, (b) $\ell = 3$, (c) $\ell = 5$ and (d) $\ell = 7$. Each graph contains curves for all the different values of $\mathcal{K}$ given in Table I.

Fig. 5). The curve for $\ell = 1$ is still separate from the rest and decays to zero at about $t = 0.1$.

Finally, for $\mathcal{K} = 0.06$, which is shown in Fig. 8(c), all the curves have merged. The trend of decaying to zero at smaller values of $\mathcal{W}$ for smaller values of $\mathcal{K}$ continues. These curves decay to zero at distances larger than the Rayleigh range $t > 1$.

From the trends in the curves in Fig. 8, we conclude that the concurrence does not in general last longer for larger values of the azimuthal index ℓ when the system constant $\mathcal{K}$ becomes smaller.

E. Parameter invariance

Although one can see from the plots in Fig. 5 that one dimensionless parameter is not enough to describe the evolution of the entanglement, they do not reveal whether or not perhaps more than two dimensionless parameters are required. For this reason, we consider different sets of dimension parameters that give the same value for $\mathcal{K}$ and plot them as a function of t. These different sets of dimension parameters are given in Table II.

Figure 9 shows five different curves of the concurrence as a function of t for $\mathcal{K} = 0.067$ and $\ell = 1$. The five curves are obtained with five different sets of dimension parameters, shown in Table II, all of which produce the same value of $\mathcal{K}$. We select $\mathcal{K} = 0.067$, because it represents a conditions where the evolution of the concurrence deviates significantly from the SPS predictions. One can see from Fig. 9 that regardless of the values of the individual dimension parameters, all the points lie on the same curve. Therefore, we conclude that the evolution of the concurrence as a function of t is completely determined by the system constant $\mathcal{K}$.

TABLE II: Dimension parameters for the curves in Fig. 9 ($\mathcal{K} = 0.067$).

Set	w_0 (m)	C_n^2 ($\mathrm{m}^{-2/3}$)	λ (nm)
1	0.100	1.0×10^{-17}	1000
2	0.176	1.0×10^{-17}	2000
3	0.100	1.0×10^{-16}	2154
4	0.035	1.0×10^{-16}	600
5	0.100	2.2×10^{-18}	600

VI. DISCUSSION

The SPS approach has been used in several studies of the effect of turbulence on the evolution of the OAM entangled bi-photon states [4–6, 8]. According to [4] the

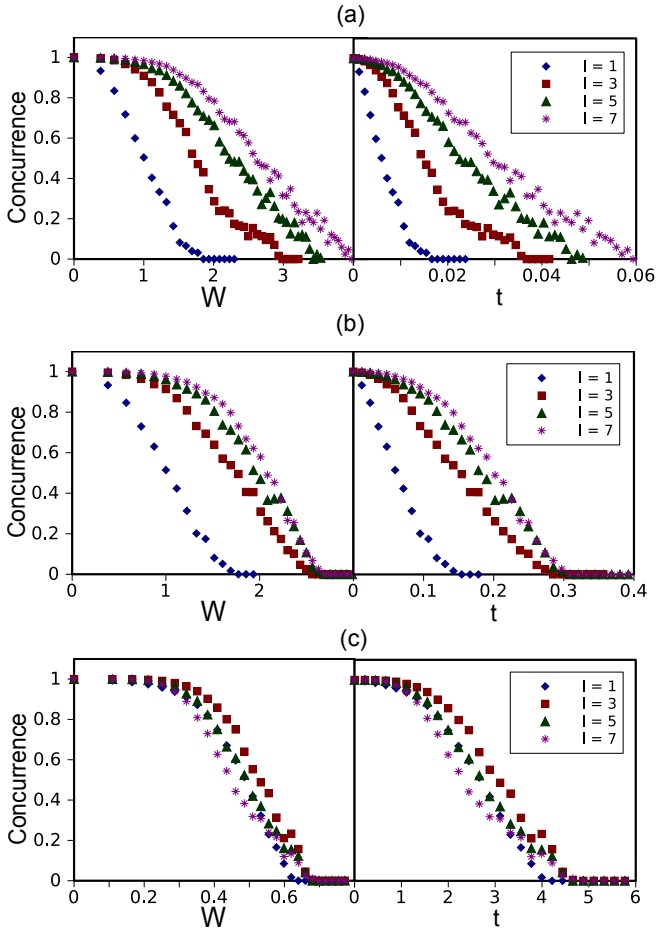

FIG. 8: The concurrence against $\mathcal{W}$ (left) and against t (right) for (a) $\mathcal{K} = 100$; (b) $\mathcal{K} = 10$; (c) $\mathcal{K} = 0.06$. Each graph contains curves for $\ell = 1, 3, 5, 7$.

evolution of the concurrence depends only on a single dimensionless quantity ($\mathcal{W} = w_0/r_0$) and the entanglement between modes with higher OAM values is more robust in turbulence. However, some important questions remained unanswered: what is the range of validity of the SPS approximation? How does the OAM entanglement evolves beyond that range?

The current study addresses these questions by using numerical simulations that represent the turbulent atmosphere with multiple phase screens. By combining all the dimension parameters (the beam radius w_0, the wavelength λ, the propagation distance z and the Kolmogorov structure constant C_n^2) into two dimensionless parameters (the normalized propagation distance t and the system constant $\mathcal{K}$), we show that the predictions made under the SPS approximation is only valid for large values of $\mathcal{K}$. Under these conditions, the concurrence decays to zero at propagation distances shorter than about a tenth of the Rayleigh range. Our results demonstrate that when $\mathcal{K}$ is large, the curves for the evolution of the concurrence tend to lie on a limiting curve that is in good

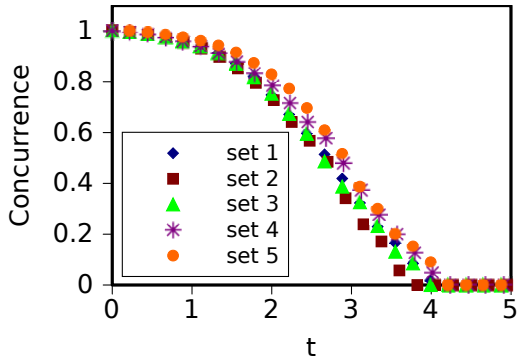

FIG. 9: Concurrence as a function of t for $\mathcal{K} = 0.067$ and $\ell = 1$, using the sets of dimension parameters given in Table II

agreement with the SPS results. Moreover, the evolution of the concurrence is fully described by the single parameter $\mathcal{W} = w_0/r_0$ and modes with larger OAM values are more robust in turbulence.

On the other hand, for weak turbulence — i.e., for small values of $\mathcal{K}$ — where the concurrence remains nonzero over propagation distances beyond one Rayleigh range, our results indicate that the evolution of the concurrence deviates significantly from the SPS predictions. Under these weaker turbulence conditions, the curves of the concurrence lie beneath the limiting curve — the decay is quicker as a function of $\mathcal{W}$ than what the SPS approach predicts. Moreover, the concurrence of modes with larger OAM values are not more robust than that of modes with smaller OAM values.

Hence, we find that in general one needs two parameters $\mathcal{K}$ and t to describe the evolution of the concurrence in turbulence conditions. This conclusion is consistent with what was found in [10].

The fact that the evolution curves for the concurrence start to deviate from the limiting curve at particular propagation distances allows us to specify a boundary that exists between the region where one can use the SPS approach and the region where one needs to employ an MPS approach. This is shown diagrammatically in Fig. 10, where we plot the Rytov variance on a vertical log scale vs the normalized propagation distance on a horizontal log scale. In this diagram, we represent the scintillation strength (Rytov variance) of an optical beam (or photon) as it propagates through particular turbulence conditions (indicated by the value of $\mathcal{K}$) by solid colored lines. The colored lines on the left-hand side represent stronger turbulence conditions than those on the right-hand side. The gray dashed lines represent the theoretical bounds (according to the SPS predictions) where the concurrence for particular values of ℓ, as indicated, vanishes. The red markers represent the points where the concurrence approaches zero as obtained form our numerical results for the different values of ℓ (red squares for $\ell = 1$, red circles for $\ell = 3$, red triangles for $\ell = 5$ and red diamonds for $\ell = 7$). The white mark-

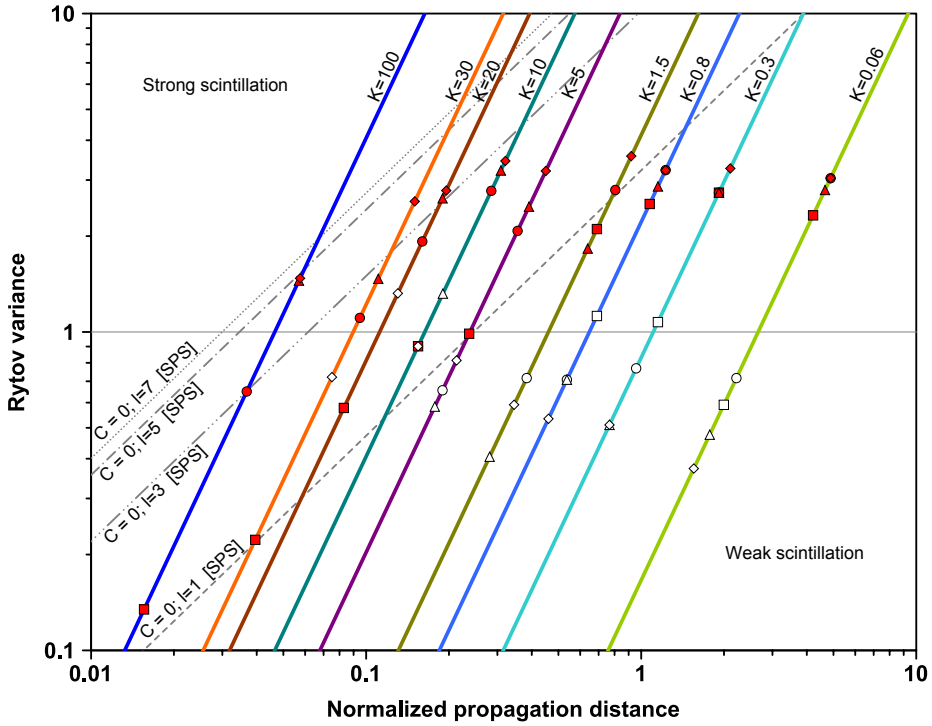

FIG. 10: The Rytov variance σ_R^2 against the normalized propagation distance t. The colored lines on the left-hand side represent stronger turbulence conditions than those on the right-hand side. The gray dashed lines are the theoretical bounds (according to the SPS approach) where the concurrence for particular values of ℓ, as indicated, will go to zero. The red markers represent the points where the concurrence vanishes for the different values of ℓ (red square for $\ell = 1$, red circle for $\ell = 3$, red triangle for $\ell = 5$ and red diamond for $\ell = 7$). The white markers represent the points where $\Delta\mathcal{C}$ exceeds a value of 0.2 for the different values of ℓ (white square for $\ell = 1$, white circle for $\ell = 3$, white triangle for $\ell = 5$ and white diamond for $\ell = 7$).

ers represent the points where the difference between the theoretical (SPS) concurrence and the numerical concurrence exceeds a value of 0.2, again for the different values of ℓ (white squares for $\ell = 1$, white circles for $\ell = 3$, white triangles for $\ell = 5$ and white diamonds for $\ell = 7$). Note that for strong enough turbulence conditions the theoretical and numerical curves never deviate more than 0.2 and thus do not produce a white marker on the diagram.

The diagram in Fig. 10 shows that the SPS approximation is valid only for $\sigma_R^2 \lesssim 0.3$. Above $\sigma_R^2 \approx 0.3$ the concurrence starts to deviate from the SPS predictions (as indicated by the general location of the white markers). One can see that on the left-hand side of the diagram, where the SPS bounds lie below $\sigma_R^2 = 1$, the points where the concurrence vanishes are still more or less located at the bounds. In contrast, on the right-hand side of the diagram, where the SPS bounds extend above $\sigma_R^2 = 1$, the points where the concurrence goes to zero are located at values of σ_R^2 that are lower than what the SPS appoximation predicts. This difference increases as one moves further right towards smaller values of the turbulence strength. In fact, judging from the highest scintillation strength where red markers are located, one can conclude that, by the time the scintillations strength increased above $\sigma_R^2 = 3$ the concurrence would always be zero, regardless of the turbulence strength.

VII. CONCLUSIONS

We presented a numerical study of the evolution of OAM entangled bi-photons propagating through atmospheric turbulence. Different values of the azimuthal index were considered. It was observed that the evolution of entanglement depends only on the dimensionless quantity $\mathcal{W} = w_0/r_0$ in the case where the scintillation strength, as quantified by the Rytov variance, is weak $\sigma_R^2 < 0.3$. For the concurrence to become zero while the beam is still in this regime, the turbulence needs to be strong. In such cases, the concurrence only lasts over propagation distances shorter than a Rayleigh range. Under these conditions, the entanglement of states with larger OAM values survives for longer distances, suggesting that states with larger OAM values are more suitable for free-space quantum communication, which agrees with what was found in previous work.

For cases where the concurrence lasts beyond the weak scintillation region — i.e., when $\sigma_R^2 > 0.3$ — the entanglement evolution depends on two dimensionless param-

eters: one is the normalized propagation distance, which is inversely proportional to the Fresnel number, and the other is a system constant that consists of the dimension parameters of the system (the beam radius w_0, the wavelength λ and the Kolmogorov structure constant C_n^2), but is independent of the propagation distance z. To reach this scintillation regime, the concurrence must remain non-zero for propagation distances greater than a Rayleigh range. In these cases the entanglement of states with higher azimuthal indices is not more robust, in contrast to cases where the scintillation is weak.

When the scintillation strength has reached $\sigma_R^2 \approx 3$ the concurrence is zero, irrespective of the turbulence strength or the azimuthal index.

Acknowledgment

The authors are grateful for the discussions with Andrew Forbes, Hermann Uys and Francesco Petruccione. This work was done with the financial support of an SRP Type A grant from the CSIR.

[1] G. W. A Mair, A Vaziri and A. Zeilinger, Nature **412**, 313 (2001).
[2] N. Gisin and R. Thew, Nat. Photonics **1**, 165 (2007).
[3] M. Mafu, A. Dudley, S. Goyal, D. Giovannini, M. McLaren, M. J. Padgett, T. Konrad, N. Petruccione, F.and Lütkenhaus, and A. Forbes, Phys. Rev. A **88**, 032305 (2013).
[4] B. J. Smith and M. G. Raymer, Phys. Rev. A **74**, 062104 (2006).
[5] A. K. Jha, G. A. Tyler, and R. W. Boyd, Phys. Rev. A **81**, 053832 (2010).
[6] G. A. Tyler and R. W. Boyd, Opt. Lett. **34**, 142 (2009).
[7] B.-J. Pors, C. H. Monken, E. R. Eliel, and J. P. Woerdman, Opt. Express **19**, 6671 (2011).
[8] A. H. Ibrahim, F. S. Roux, M. McLaren, T. Konrad, and A. Forbes, Phys. Rev. A **88**, 012312 (2013).
[9] C. Paterson, Phys. Rev. Lett. **94**, 153901 (2005).
[10] F. S. Roux, Phys. Rev. A **83**, 053822 (2011).
[11] F. S. Roux, Phys. Rev. A **88**, 049906 (2013).
[12] F. S. Roux, J. Phys. A: Math. Theor. **47**, 195302 (2014).
[13] A. N. Kolmogorov, C. R. (Doki) Acad. Sci. U.S.S.R. **30**, 301 (1922).
[14] L. C. Andrews and R. L. Phillips, *Laser Beam Propagation Through Random Media* (SPIE, Washington, 1998).
[15] W. K. Wootters, Phys. Rev. Lett. **80**, 2245 (1998).
[16] J. M. Martin and S. M. Flatté, Appl. Opt. **27**, 2111 (1988).
[17] J. M. Martin and S. M. Flatté, J. Opt. Soc. Am. A **7**, 838 (1990).
[18] T. Konrad, F. de Melo, M. Tiersch, C. Kasztelan, A. Aragao, and A. Buchleitner, Nature Physics **4**, 99 (2007).
[19] M. Tiersch, F. de Melo, and A. Buchleitner, Phys. Rev. Lett. **101**, 170502 (2008).
[20] M. Tiersch, F. Melo, T. Konrad, and A. Buchleitner, Q. Inf. Proc. **8**, 523 (2009).
[21] G. Gour, Phys. Rev. Lett. **105**, 190504 (2010).
[22] S. M. Wandzura, J. Opt. Soc. Am. **70**, 745 (1980).